



Title	Air-stable and reusable nickel phosphide nanoparticle catalyst for the highly selective hydrogenation of d-glucose to d-sorbitol
Author(s)	Yamaguchi, Sho; Fujita, Shu; Nakajima, Kiyotaka et al.
Citation	Green Chemistry. 2021, 23(5), p. 2010-2016
Version Type	AM
URL	https://hdl.handle.net/11094/79298
rights	
Note	

The University of Osaka Institutional Knowledge Archive : OUKA

<https://ir.library.osaka-u.ac.jp/>

The University of Osaka

FULL PAPER

Air-stable and reusable nickel phosphide **nanoparticle** catalyst for the highly selective hydrogenation of D-glucose to D-sorbitol

Received 00th January 20xx,
Accepted 00th January 20xx

Sho Yamaguchi,^a Shu Fujita,^a Kiyotaka Nakajima,^b Seiji Yamazoe,^c Jun Yamasaki,^d Tomoo Mizugaki^a and Takato Mitsudome^{*a}

DOI: 10.1039/x0xx00000x

The hydrogenation of carbohydrates to polyols is an industrially important process, but it requires air-unstable, non-noble metal catalysts with low activity and harsh reaction conditions. Herein, we report a hydrotalcite (HT)-supported nickel phosphide **nanoparticle** (nano-Ni₂P/HT) that exhibits both air stability and high activity for the selective hydrogenation of D-glucose to D-sorbitol in water. The nano-Ni₂P/HT catalyst provides D-sorbitol in excellent yield with >99% selectivity under mild reaction conditions, and is the first non-noble metal catalyst that can operate under just 1 bar of H₂ or at ambient temperature. This high-performance nano-Ni₂P/HT catalyst is significantly different from conventional Ni(0) and NiO nanoparticles and Raney catalysts, which result in almost no production of D-sorbitol, demonstrating the unique catalysis of nano-Ni₂P/HT. Furthermore, nano-Ni₂P/HT shows the highest activity among those reported for non-noble metal catalysts. The nano-Ni₂P/HT catalyst can also be reused without sacrificing its high activity and selectivity. Additionally, the successful transformation of a concentrated D-glucose solution (50 wt%) to D-sorbitol has been achieved. This is the first example of an air-stable, highly active, and reusable non-noble metal catalyst that can replace conventional catalysts used for D-sorbitol production, thus providing a cheap, green, and sustainable route for this process.

Introduction

D-Sorbitol is a large-volume sugar alcohol that is ubiquitous and widely applied in numerous fields, including food and cosmetic industries and drug synthesis.¹ It can also be used as a starting material for the synthesis of various useful products, such as L-ascorbic acid and lower polyols, which are downstream products in the petrochemical industry.² The versatility of D-sorbitol has promoted its inclusion in the list of the top ten biomass-derived building blocks that can be converted into high-value, bio-based products or materials.³

The catalytic hydrogenation of D-glucose^{4–6} is a reliable and straightforward method for synthesizing D-sorbitol with a production rate of more than 800,000 ton y^{–1}. This reaction has been well studied using various heterogeneous catalysts comprising Ni,^{2,7–20} Co,^{18,21–23} Rh,⁸ Ru,^{13,24–37} or Pt.^{35,38,39} Among them, sponge Ni catalysts, such as Raney Ni, are predominantly used for industrial D-sorbitol production because they are

composed of low-cost, earth-abundant elements. However, sponge Ni catalysts suffer from pyrophoricity⁴⁰ and undergo rapid deactivation caused by metal leaching, metal sintering, and support degradation.^{41,42} Moreover, owing to their low catalytic activities, high hydrogen gas pressures and temperatures (100–180 °C and under 50–150 bar⁶, respectively) are inevitably required. As an alternative to Ni-based catalysts, noble-metal-based catalysts, such as carbon-supported Ru catalysts, have been recently developed for D-sorbitol production.^{25,27,29,31,33–36} Although these catalysts are efficient, their constituent metals are rare and expensive. Furthermore, these catalysts are susceptible to poisoning by strong coordination with organic impurities.⁴³ Consequently, from the perspectives of practicality and green sustainable chemistry, the development of air-stable, highly active, and reusable non-noble metal catalysts for D-glucose hydrogenation is an extremely important goal.

Recently, our group has reported the unique catalysis of a Ni phosphide **nanoparticle (NP)** (nano-Ni₂P) to promote the selective transformation of biofuranic aldehydes to diketones in water.⁴⁴ Unlike the conventional sponge Ni catalysts, nano-Ni₂P has an air-stable metallic nature without pyrophoricity and shows high hydrogenation activity comparable to that of noble-metal catalysts. These facts encouraged us to employ nano-Ni₂P as a green catalytic system for the hydrogenation of D-glucose to D-sorbitol. Herein, we report the highly efficient catalytic transformation of D-glucose into D-sorbitol using supported nano-Ni₂P catalysts. A hydrotalcite (HT; Mg₆Al₂(OH)₁₆CO₃·4H₂O)-supported Ni₂P **NP** (nano-Ni₂P/HT) exhibited both air stability and high activity for the

^a Department of Materials Engineering Science, Graduate School of Engineering Science, Osaka University, 1-3 Machikaneyama, Toyonaka, Osaka 560-8531, Japan. E-mail: mitsudome@cheng.es.osaka-u.ac.jp

^b Institute for Catalysis, Hokkaido University, Kita 21 Nishi 10, Kita-ku, Sapporo 001-0021, Japan

^c Department of Chemistry, Tokyo Metropolitan University, 1-1 Minami Osawa, Hachioji, Tokyo 192-0397, Japan

^d Research Center for Ultra-High Voltage Electron Microscopy, Osaka University, 7-1, Mihogaoka, Ibaraki, Osaka 567-0047, Japan

Electronic Supplementary Information (ESI) available: General experimental details, characterization of fresh and spent Ni₂P catalysts, gram-scale and recycling experiments, performance comparison with previously reported catalysts. See DOI: 10.1039/x0xx00000x

hydrogenation of D-glucose in water under mild reaction conditions (1 bar of H₂ or ambient temperature). Notably, the achieved turnover number (TON) was higher than those of previously reported non-noble metal catalysts. This outstanding performance significantly distinguished nano-Ni₂P/HT from other conventional Ni catalysts, such as Ni(0) and NiO NPs, and Raney catalysts. Furthermore, nano-Ni₂P/HT could be recycled without losing its original activity and was successfully applied to the high-yield synthesis of D-sorbitol from a concentrated D-glucose solution (50 wt%), thus demonstrating the significant potential of this catalyst for industrial applications.

Experimental

Reagents

Nickel(II) acetylacetonate (Ni(acac)₂, 95%) was purchased from Sigma-Aldrich (Japan), whereas >97% triphenyl phosphite and >95% hexadecylamine were purchased from Tokyo Chemical Industry Co. Ltd. (Japan). All the employed organic reagents were purified before use. HT (AD-500NS) was obtained from Tomita Pharmaceutical Co. Ltd. (Japan) and SiO₂ (Q-6) was procured from Fuji Silysia Chemicals (Japan). TiO₂ (JRC TIO-15) and ZrO₂ (JRC ZRO-6) were provided by the Catalysis Society of Japan and used as reference catalyst supports. Al₂O₃ (AKP-G015) was obtained from Sumitomo Chemical Co. Ltd. (Japan). Nb₂O₅ and Y₂O₃ were purchased from Wako Pure Chemical Industries Ltd. (Japan). Ru/C and mordenite were obtained from N.E. CHEMCAT and the Catalysis Society of Japan, respectively. Raney Ni (~50%) was obtained from Wako Pure Chemical Industries Ltd. (Japan).

Characterization

Inductively coupled plasma atomic emission spectrometry (ICP-AES) was performed using an SII Nano Technology SPS7800 instrument. Transmission electron microscopy (TEM) was conducted on JEM-ARM200F and FEI Tecnai G2 20ST instruments operating at 200 kV. The size distributions were determined by counting 200 particles. Scanning transmission electron microscopy (STEM) images and corresponding energy-dispersive X-ray spectroscopy (EDX) data were collected using an FEI Titan Cubed G2 60-300 instrument operating at 300 kV and equipped with a Super-X EDX detector. Elemental mapping based on the quantitative analysis of the EDX spectra was carried out using Esprit software. Ni K-edge X-ray absorption spectra were recorded at room temperature using a Si (111) monochromator at the BL01B1 and BL14B2 lines of SPring-8 at the Japan Synchrotron Radiation Research Institute (JASRI) in Harima, Japan. The obtained spectra were analyzed using Athena software. After normalization at the edge height, the *k*³-weighted χ spectra were extracted. Subsequently, these spectra in the *k* range of 3–13 Å^{−1} were Fourier-transformed (FT) into the *R*-space. Curve-fitting analysis was conducted in the *R* range of 1.3–2.7 Å using the back-scattering amplitude and phase shift functions of Ni–P and Ni–Ni, which were calculated with the FEFF8.5L program.⁴⁵ X-ray diffraction (XRD) patterns were recorded using a Philips X'Pert-MPD diffractometer with Cu-K α

radiation. X-ray photoelectron spectroscopy (XPS) analysis was performed on a KRATOS system equipped with a mono Al X-ray source and a hemispherical analyzer operating in the fixed analyzer transmission mode. The spectra were obtained at a pass energy of 40.0 eV with an Al–K X-ray source operating at 50 W and 154 kV. The analysis area was 0.7 × 0.3 mm² and the working pressure in the analysis chamber was less than 1 × 10^{−8} Pa. The C 1s peak at a binding energy of 284.6 eV was used as the internal reference.

Catalyst Preparation

All the experiments were conducted using standard Schlenk line techniques. nano-Ni₂P was prepared according to our previous report⁴⁴ with some modifications. Ni(acac)₂ (1.0 mmol) and hexadecylamine (10 mmol) were combined with triphenyl phosphite (10 mmol) in a Schlenk flask. The mixture was stirred at 120 °C for 1 h in vacuo, heated to 315 °C at a rate of 30 °C min^{−1}, and then kept constant for 2 h, yielding a black colloidal solution. After cooling the mixture to room temperature, the black product was isolated by precipitation in acetone. The obtained precipitate was washed several times with a chloroform–acetone mixture and then dried in vacuo overnight to afford nano-Ni₂P. Next, nano-Ni₂P (23 mg) was dispersed in hexane (50 mL) via sonication for 1 h and then stirred with HT (1.0 g) for 6 h at room temperature to afford nano-Ni₂P/HT as a gray powder. A similar procedure was followed to prepare the other nano-Ni₂P/support catalysts. Ni/HT and its H₂-reduced form (Ni/HT-Red) were used as model catalysts for NiO NPs and Ni(0) NPs, respectively, and were prepared as follows: Ni(acac)₂ (0.3 mmol) was added to acetone (50 mL) with stirring. After 10 min, HT (1.0 g) was added and the mixture was stirred for 1 h. Acetone was then removed by evaporation under reduced pressure to give a pale green powder. The obtained powder was dried in vacuo overnight and calcined in air at 500 °C for 3 h to give Ni/HT. Then, Ni/HT was treated with a H₂ flow at 600 °C for 3 h^{46,47} to afford Ni/HT-Red. A TEM image and the XPS analysis of Ni/HT-Red are shown in Figs. S1 and S2, respectively. The Ni(0) NPs approximately 5.0 nm in diameter were highly dispersed on HT.

Reaction procedure

D-glucose (90 mg, 0.5 mmol), supported Ni₂P catalyst (200 mg, 33 μ mol Ni), and distilled water (3 mL) were placed in a 50 mL stainless-steel autoclave with a Teflon inner cylinder. The reactor was purged four times with H₂ and pressurized with 20 bar of H₂ at room temperature. The reactor was then heated at 100 °C for 2 h while stirring at 800 rpm. After the reaction, the autoclave was cooled in an ice-water bath and the H₂ gas was carefully released. The reaction mixture was subsequently separated by centrifugation. The products in solution were analyzed by high-performance liquid chromatography (HPLC; Shimadzu LC-20AD, refractive index detector) using a Phenomenex Rezex RPM-Monosaccharide Pb⁺⁺ column (ϕ = 7.8 × 300 mm; mobile phase: water, 0.6 mL min^{−1}, 70 °C). The conversion of D-glucose and the yield of D-sorbitol were determined by HPLC analysis using D-sucrose as an internal standard.

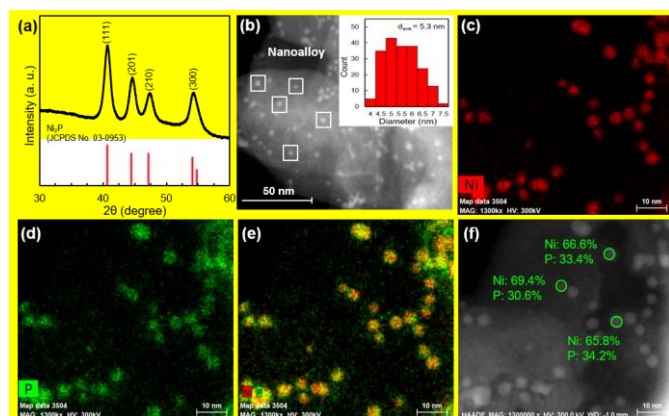


Fig. 1 (a) X-ray diffraction (XRD) patterns of nano- Ni_2P and the Ni_2P reference (JCPDS No. 03-0953); (b) High-angle annular dark-field scanning transmission electron microscopy (HAADF-STEM) image and size distribution histogram (inset) of nano- Ni_2P /hydrotalcite (HT); elemental mapping of (c) Ni and (d) P; (e) composite overlay of (c) and (d); and (f) energy-dispersive X-ray spectroscopy (EDX) analysis of nano- Ni_2P /HT in the regions indicated by green circles.

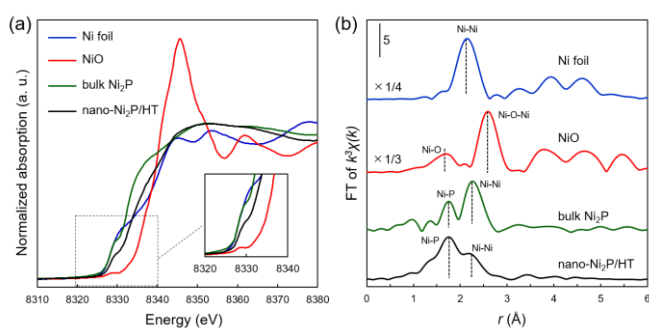


Fig. 2 (a) Ni K-edge X-ray absorption near-edge structure (XANES) spectra and (b) Fourier-transformed (FT) k^2 -weighted extended X-ray absorption fine structure (EXAFS) spectra of Ni foil, NiO, bulk Ni_2P , and nano- Ni_2P /HT.

Results and discussion


Catalyst characterization studies

The crystal structure of pristine nano- Ni_2P was evaluated by XRD (Fig. 1a). The diffraction peaks were consistent with those of bulk Ni_2P and could be indexed to the hexagonal Ni_2P phase.⁴⁸ The weak and broad diffraction peaks suggested the formation of nanosized Ni_2P . The representative high-angle annular dark-field (HAADF)-STEM image of nano- Ni_2P /HT in Fig. 1b reveals the formation of spherical nano- Ni_2P with a mean diameter of 5.3 nm (Fig. 1b inset). The XRD pattern of nano- Ni_2P /HT exhibits peaks attributed to the HT structure, while no peaks corresponding to Ni species are observed due to the high dispersion of the small Ni_2P NPs on HT (Fig. S3). The loading amount of Ni was determined to be 0.89 wt% by ICP-AES analysis. Furthermore, HAADF-STEM coupled with EDX showed that Ni and P are homogeneously dispersed in nano- Ni_2P , where the molar ratio of Ni to P was $\sim 2:1$ (Figs. 1c–f). Overall, these results support the successful synthesis of nano- Ni_2P /HT, which consists of spherical nano- Ni_2P highly dispersed on the HT surface.

Next, X-ray absorption fine structure (XAFS) analysis was carried out to elucidate the electronic state of the Ni species in nano- Ni_2P /HT. The X-ray absorption near-edge structure (XANES) spectrum of nano- Ni_2P /HT was compared to those of Ni foil, NiO, and bulk Ni_2P as references (Fig. 2a). The absorption edge energy of nano- Ni_2P /HT was similar to that of Ni foil, suggesting that the Ni species in nano- Ni_2P /HT exists in a metal-like state, even after exposure to air. This result agrees with the conclusions of the XPS analysis of nano- Ni_2P /HT, where two peaks observed at 852.4 and 869.4 eV are very similar to those of metallic Ni $2p_{3/2}$ (852.8 eV) and Ni $2p_{1/2}$ (870.0 eV), respectively (Fig. S4a). This unique air stability distinguishes nano- Ni_2P /HT from pyrophoric sponge Ni catalysts and conventional air-unstable Ni NP catalysts. The P 2p spectrum shows two peaks, indicating the coexistence of phosphorus atoms with different electronic states on the surface of the Ni_2P NPs (Fig. S4b). The first peak at 129.2 eV is close to that of P^0 (130.0 eV) and assigned as $\text{P}^{\delta-}$ ($0 < \delta < 1$), while the other peak at 132.3 eV is assigned to the PO_4^{3-} phosphate species arising from the superficial oxidation of the Ni_2P NPs. These results demonstrate that the Ni species in the Ni_2P NPs possess metallic states in air. Fig. 2b shows the FT-extended XAFS (FT-EXAFS) spectrum of nano- Ni_2P /HT along with those of Ni foil, NiO, and bulk Ni_2P as references. The spectrum of nano- Ni_2P /HT displays peaks corresponding to Ni–P and Ni–Ni bonds, which are observed at 1.7–2.0 and 2.0–2.5 Å, respectively. The absence of peaks corresponding to Ni–O bonds indicates that nano- Ni_2P /HT is not oxidized in air. The curve-fitting analysis of the EXAFS spectra is shown in Fig. S5 and the results are summarized in Table S1. The Ni–Ni bond (2.57 Å) of nano- Ni_2P /HT was longer than that of Ni foil (2.48 Å) owing to its network of NiP_4 tetrahedra that share vertices. In addition, the $CN_{\text{Ni-Ni}}/CN_{\text{Ni-P}}$ ratio (0.9) of nano- Ni_2P /HT was much lower than that of the ideal value in bulk Ni_2P (3.3), indicating that coordinatively unsaturated Ni atoms exist on the Ni_2P surface in nano- Ni_2P /HT. The lower $CN_{\text{Ni-Ni}}/CN_{\text{Ni-P}}$ ratio of nano- Ni_2P /HT may be due to the exposure of large amounts of Ni atoms (Ni(2)) along the (300) plane, as shown in Fig S3. In addition, the Ni–P bonds (Ni(1)–P in Fig. S6) were more rigid than the Ni–Ni bonds (Ni(1)–Ni(2)) because the latter exhibited a large Debye–Waller (DW) factor (DW > 0.01, Table S1). Therefore, coordinatively unsaturated Ni(2) sites are formed on the nano- Ni_2P /HT surface.

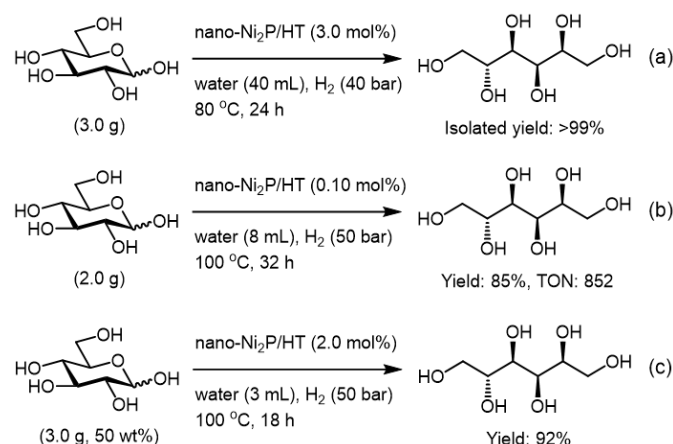
Catalytic performance of nano- Ni_2P /HT

We investigated the catalytic activities of nano- Ni_2P supported on various metal oxides for the hydrogenation of D-glucose in water at 100 °C under 20 bar of H_2 , and the results are summarized in Table 1. Notably, HT-supported nano- Ni_2P showed a high activity, providing D-sorbitol in 99% yield (entry 1). Other oxide supports, such as Al_2O_3 , ZrO_2 , and Y_2O_3 , were also effective for D-sorbitol production, but the yields were lower than that obtained with nano- Ni_2P /HT (entries 2–4). Furthermore, the use of TiO_2 , Nb_2O_5 , SiO_2 , and mordenite provided low D-glucose conversions (entries 5–8). These results reveal that the combination of the nano- Ni_2P and HT provided the best catalytic performance for D-glucose hydrogenation.

Table 1 Hydrogenation of D-glucose using supported nano-Ni₂P catalysts.^a


Entry	Catalyst	H ₂ [bar]	Temp. [°C]	Time [h]	D-Glucose conv. [%] ^b	D-Sorbitol yield [%] ^b	D-Mannitol yield [%] ^b
1	nano-Ni ₂ P/HT	20	100	2	>99	99	1
2	nano-Ni ₂ P/Al ₂ O ₃	20	100	2	83	78	1
3	nano-Ni ₂ P/ZrO ₂	20	100	2	65	43	4
4	nano-Ni ₂ P/Y ₂ O ₃	20	100	2	49	42	<1
5	nano-Ni ₂ P/TiO ₂	20	100	2	20	4	<1
6	nano-Ni ₂ P/Nb ₂ O ₅	20	100	2	18	13	<1
7	nano-Ni ₂ P/SiO ₂	20	100	2	11	8	<1
8	nano-Ni ₂ P/mordenite	20	100	2	6	3	<1
9	Ni/HT	20	100	2	83	1	<1
10	Ni/HT-Red	20	100	2	84	<1	<1
11	Raney Ni	20	100	2	4	4	<1
12	Ru/C	20	100	2	>99	88	8
13	nano-Ni ₂ P/HT ^c	50	25	72	90	90	<1
14	nano-Ni ₂ P/HT	10	100	2	94	88	5
15	nano-Ni ₂ P/HT	1	100	12	>99	73	5

^a Reaction conditions: catalyst (6.6 mol% Ni or Ru), D-glucose (0.5 mmol), water (3 mL). ^b Conversion of D-glucose and yield of D-sorbitol were determined by HPLC analysis based on an internal standard method. ^c Catalyst (13 mol% Ni).

**Scheme 1** Gram-scale experiments with (a) 3.0 mol% and (b) 0.10 mol% nano-Ni₂P/HT. (c) Hydrogenation of D-glucose at a concentration of 50 wt%.

In control experiments, conventional Ni catalysts Ni/HT and Ni/HT-Red were tested as model catalysts for NiO NPs and Ni(0) NPs, respectively, in the hydrogenation of D-glucose. Both Ni/HT and Ni/HT-Red gave negligible amounts of D-sorbitol and undetectable by-products (entries 9 and 10). Raney catalysts, which are considered state-of-the-art hydrogenation catalyst systems, are often employed for D-glucose hydrogenation. Under the above reaction conditions, Raney Ni displayed poor activity, providing D-sorbitol in only 4% yield (entry 11), which demonstrates that the nano-Ni₂P/HT catalyst outperforms Raney catalysts and other conventional Ni catalysts. Interestingly, the D-sorbitol yield obtained with the nano-Ni₂P/HT catalyst was also higher than that provided by a

commercially available noble-metal catalyst (Ru/C), which formed mannitol in 8% yield as an undesired byproduct (entries 1 and 12). Thus, nano-Ni₂P/HT shows catalytic activity for this reaction that is superior to that of conventional noble-metal-based catalysts. The high performance of nano-Ni₂P/HT was further highlighted in the hydrogenation of D-glucose under milder conditions. Even at room temperature, nano-Ni₂P/HT afforded D-sorbitol in 90% yield (entry 13), whereas there have been no previous reports on D-glucose hydrogenation at temperatures below 90 °C (Table S2). Furthermore, nano-Ni₂P/HT promoted the hydrogenation of D-glucose under lower H₂ pressures (10 and 1 bar) to afford D-sorbitol in 88% and 73% yields, respectively (entries 14 and 15), thus outperforming previously reported catalysts that require 20–50 bar^{9,10,13–23} or 120 bar^{11,12} of H₂ (Table S2). To the best of our knowledge, nano-Ni₂P/HT is the first successful non-noble metal catalyst for the hydrogenation of D-glucose operating at ambient temperature and under an atmospheric pressure of H₂.

The nano-Ni₂P/HT catalyst was applicable to the gram-scale production of D-sorbitol in water, where 3.0 g of D-glucose was quantitatively converted to D-sorbitol in >99% isolated yield (Scheme 1a, Fig. S7). When the hydrogenation was examined with low amounts of nano-Ni₂P/HT (0.10 mol%, Scheme 1b), D-sorbitol was obtained in 85% yield with a TON exceeding 852. This value is the highest among those previously reported for non-noble metal catalysts (Table S2). As D-sorbitol production from a concentrated D-glucose solution is a challenge facing most practical applications of this process, we investigated the operability of our nano-Ni₂P/HT catalyst in a 50 wt% D-glucose solution, which resulted in D-sorbitol being produced in 92% yield (Scheme 1c). This result clearly demonstrates the great

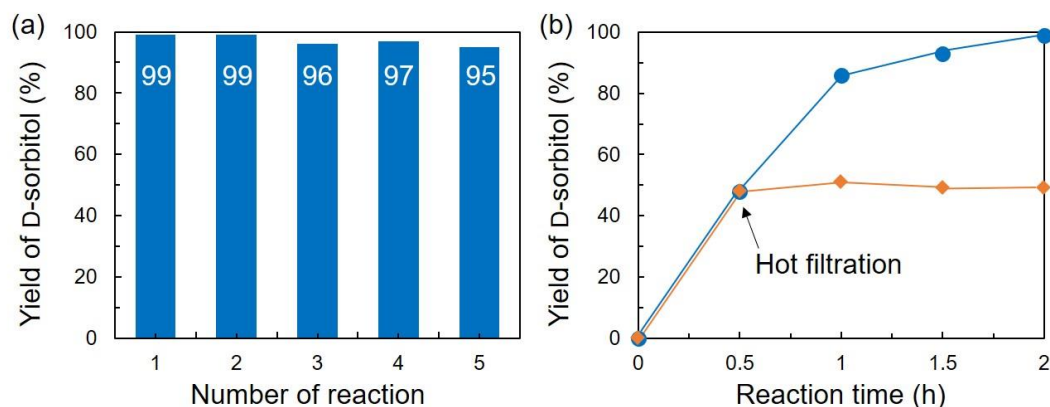


Fig. 3 (a) Reusability of nano-Ni₂P/HT for the hydrogenation of D-glucose. Reaction conditions: nano-Ni₂P/HT (6.6 mol% Ni), D-glucose (0.5 mmol), water (3 mL), H₂ (20 bar), 100 °C, 2 h. (b) Time course of the hydrogenation of D-glucose using nano-Ni₂P/HT: (●) without catalyst removal and (●) with catalyst removal by hot filtration after 0.5 h. Reaction conditions: nano-Ni₂P/HT (6.6 mol% Ni), D-glucose (0.5 mmol), water (3 mL), H₂ (20 bar), 100 °C.

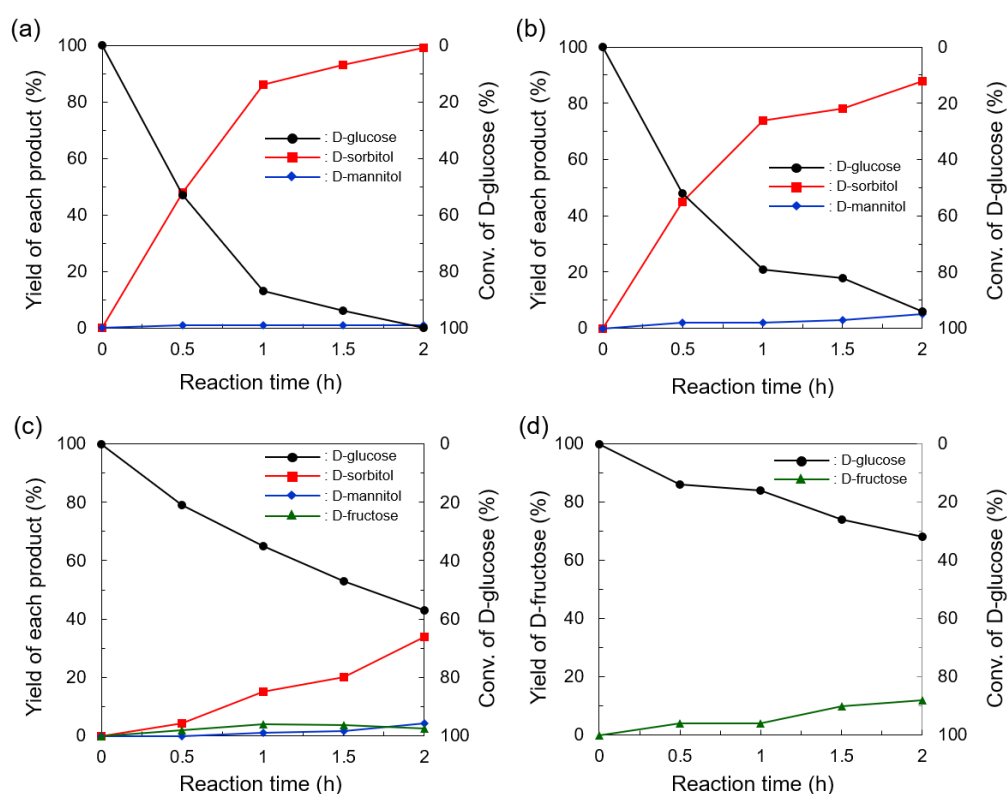


Fig. 4 (a–c) Time courses of the hydrogenation of D-glucose using nano-Ni₂P/HT. Reaction conditions: nano-Ni₂P/HT (6.6 mol% Ni), D-glucose (0.5 mmol), water (3 mL), 100 °C, H₂ ((a) 20 bar, (b) 10 bar, and (c) 1 bar). (d) D-Glucose isomerization over HT support. Reaction conditions: HT (200 mg), D-glucose (0.5 mmol), water (3 mL), 100 °C, N₂ (1 bar).

potential of this catalyst for industrial applications.

Next, the reusability of nano-Ni₂P/HT was investigated. After the hydrogenation, nano-Ni₂P/HT was recovered by centrifugation and reused for the next reaction without any pretreatment. The experiment was repeated four times and no significant decreases were observed in either the D-sorbitol yield or D-glucose conversion (Fig. 3a). The reusability of nano-Ni₂P/HT is distinct from that of reported non-noble metal catalysts, such as Raney Ni,² Ni–Co,¹⁸ and Ni/NiO¹⁹ catalysts,

where the activity decreases upon recycling owing to surface poisoning by polymerized byproducts or leaching of the Ni metal. Therefore, we also evaluated the leaching of the metal species during the reaction (Fig. 3b). After 0.5 h of the hydrogenation reaction, the nano-Ni₂P/HT catalyst was removed by filtration and the filtrate was then treated under the same hydrogenation conditions. Further heat treatment of the filtrate for 1.5 h did not produce additional D-sorbitol. Furthermore, based on ICP-AES analyses of the fresh and spent

catalysts, Ni loading amounts were not changed, confirming that almost no Ni species were leached from the catalyst. These results indicate that nano-Ni₂P is strongly immobilized on the HT support and that the hydrogenation of D-glucose is attributed to heterogeneous catalysis. Structural analyses before and after the reaction were carried out using XPS, TEM, and EDX. From the XPS analysis, we noted that the binding energy peaks of the spent nano-Ni₂P/HT were almost identical to those of the fresh nano-Ni₂P/HT (Fig. S4 vs S8, respectively). This clearly shows that the Ni₂P NPs on the HT support have an air-stable metallic nature even after the hydrogenation of D-glucose. The TEM image of nano-Ni₂P/HT after the reaction also confirmed that the spherical shape of nano-Ni₂P was preserved (Fig. S9). HAADF-STEM coupled with EDX revealed that the molar ratio of Ni to P in nano-Ni₂P/HT after the reaction was ~2:1, similar to that of fresh nano-Ni₂P/HT (Fig. S10). These results clearly verify that nano-Ni₂P/HT is highly durable, which is consistent with the high reusability observed for this catalyst.

Rationalization of the catalytic behavior of nano-Ni₂P/HT based on time-course experiments

To gain more insight into the catalytic features of nano-Ni₂P/HT, time-course measurements were carried out at 100 °C under 20, 10, and 1 bar of H₂. A quantitative amount of D-sorbitol was obtained under 20 bar of H₂ (Fig. 4a), whereas small amounts of D-fructose and its hydrogenated product, D-mannitol, were observed under 10 and 1 bar of H₂ (Figs. 4b and 4c). It has been reported that HT efficiently promotes the isomerization of D-glucose to D-fructose.⁴⁹ Therefore, these byproducts were likely formed by HT catalysis. In fact, HT provided D-fructose under our experimental conditions (HT, water, 1 bar of N₂, 100 °C) (Fig. 4d). On the other hand, HT is also known to have oxygen vacancies on its surface, which act as Lewis acid sites for the activation of carbonyl moieties.⁵⁰ These facts suggest that HT plays a dual role in the present D-glucose hydrogenation system. Namely, HT can activate the carbonyl moiety of the D-glucose aldehyde group, which facilitates the selective production of D-sorbitol (positive effect) while causing the undesired isomerization of D-glucose to D-fructose (negative effect). The positive effect of the HT support for facilitating the Ni₂P-catalyzed hydrogenation becomes remarkable at higher H₂ pressures, thus giving priority to D-sorbitol production through a cooperative effect between nano-Ni₂P and HT.

Conclusions

We report that an HT-supported Ni₂P NP can serve as a smart heterogeneous catalyst for the high-yield synthesis of D-sorbitol from D-glucose. In sharp contrast to conventional air-unstable catalysts with low activity, our nano-Ni₂P catalyst exhibited both air stability and high activity under mild conditions. Furthermore, nano-Ni₂P outperformed conventional Ni catalysts, including Ni(0) and NiO NPs, and Raney Ni and exhibited the highest activity among those previously reported for non-noble metal catalysts. Moreover, nano-Ni₂P/HT successfully operates under just 1 bar of H₂ or at ambient temperature. Upon undergoing repeated recycling, nano-

Ni₂P/HT retained its high activity and selectivity and operated well in a concentrated D-glucose solution, clearly representing the great potential of this catalyst for industrial applications. We believe that nano-Ni₂P/HT, with its excellent air stability, high activity, and reusability, could serve as a green alternative to conventional industrial catalysts (e.g., sponge Ni catalysts). This inexpensive and efficient non-noble metal phosphide catalyst will make a significant contribution to the development of future, sustainable reaction processes.

Conflicts of interest

There are no conflicts to declare.

Acknowledgements

This work was supported by JSPS KAKENHI Grant Nos. 17H03457, 17H03456, 18H01790, and 20H02523. This study was partially supported by the Cooperative Research Program of the Institute for Catalysis, Hokkaido University (20B1027). A part of this work was supported by the "Nanotechnology Platform" Program at Hokkaido University (A-20-HK-0011) and Nanotechnology Open Facilities in Osaka University (A-19-OS-0060) of the Ministry of Education, Culture, Sports, Science and Technology (MEXT), Japan. We thank Dr. Toshiaki Ina (SPRING-8) for XAFS measurements (2019A1390, 2019A1649, 2019B1560, and 2020A1487) and Ryo Ota of Hokkaido University for STEM analysis.

References

- O. Casanova, S. Iborra and A. Corma, *ChemSusChem*, 2009, **2**, 1138–1144.
- P. Gallezot, P. J. Cerino, B. Blanc, G. Flèche and P. Fuertes, *J. Catal.*, 1994, **146**, 93–102.
- J. J. Bozell and G. R. Petersen, *Green Chem.*, 2010, **12**, 539–554.
- A. Corma, S. Iborra and A. Velty, *Chem. Rev.*, 2007, **107**, 2411–2502.
- J. Song, H. Fan, J. Ma and B. Han, *Green Chem.*, 2013, **15**, 2619–2635.
- M. Besson, P. Gallezot and C. Pinel, *Chem. Rev.*, 2014, **114**, 1827–1870.
- P. H. Brahme and L. K. Doraiswamy, *Ind. Eng. Chem. Process Des. Dev.*, 1976, **15**, 130–137.
- J. Wisnlak and R. Simon, *Ind. Eng. Chem. Prod. Res. Dev.*, 1979, **18**, 50–57.
- H. Li, W. Wang and J. F. Deng, *J. Catal.*, 2000, **191**, 257–260.
- H. Li, H. Li and J.-F. Deng, *Catal. Today*, 2002, **74**, 53–63.
- B. Kusserow, S. Schimpf and P. Claus, *Adv. Synth. Catal.*, 2003, **345**, 289–299.
- S. Schimpf, C. Louis and P. Claus, *Appl. Catal. A*, 2007, **318**, 45–53.
- J. Zhang, L. Lin, J. Zhang and J. Shi, *Carbohydr. Res.*, 2011, **346**, 1327–1332.
- J. Guo, Y. Hou, C. Yang, Y. Wang, H. He and W. Li, *Catal. Commun.*, 2011, **16**, 86–89.
- J. Guo, Y. Hou, C. Yang, Y. Wang and L. Wang, *Mater. Lett.*, 2012, **67**, 151–153.
- J. Zhang, S. Wu, Y. Liu and B. Li, *Catal. Commun.*, 2013, **35**, 23–26.

- 17 R. Rodiansono and S. Shimazu, *Bull. Chem. React. Eng. Catal.*, 2013, **8**, 40–46.
- 18 Q. Dong, Y. Huang, H. Yang, J. Pei, K. Li, M. Yuan, W. Xiao, W. Ni and Z. Hou, *Top. Catal.*, 2017, **60**, 666–676.
- 19 H. Singh, A. Rai, R. Yadav and A. K. Sinha, *Mol. Catal.*, 2018, **451**, 186–191.
- 20 Y. Yang, H. Gu, Q. Zhang, H. Li and H. Li, *ACS Appl. Mater. Interfaces*, 2020, **12**, 26101–26112.
- 21 H. Li, H. Li, W. Wang and J.-F. Deng, *Chem. Lett.*, 1999, **28**, 629–630.
- 22 H. Li, H. Li and M. Wang, *Appl. Catal. A*, 2001, **207**, 129–137.
- 23 H. Li and J.-F. Deng, *J. Chem. Technol. Biotechnol.*, 2001, **76**, 985–990.
- 24 P. Gallezot, N. Nicolaus, G. Flèche, P. Fuertes and A. Perrard, *J. Catal.*, 1998, **180**, 51–55.
- 25 K. van Gorp, E. Boerman, C. V. Cavenaghi and P. Berben, *Catal. Today*, 1999, **52**, 349–361.
- 26 H. Guo, H. Li, Y. Xu and M. Wang, *Mater. Lett.*, 2002, **57**, 392–398.
- 27 B. W. Hoffer, E. Crezee, P. R. M. Mooijman, A. D. van Langeveld, F. Kapteijn and J. A. Moulijn, *Catal. Today*, 2003, **79–80**, 35–41.
- 28 E. P. Maris, W. C. Ketchie, V. Oleshko and R. J. Davis, *J. Phys. Chem. B*, 2006, **110**, 7869–7876.
- 29 J. Liu, P. Bai and X. S. Zhao, *Phys. Chem. Chem. Phys.*, 2011, **13**, 3758–3763.
- 30 D. K. Mishra, J.-M. Lee, J.-S. Chang and J.-S. Hwang, *Catal. Today*, 2012, **185**, 104–108.
- 31 V. N. Sapunov, M. Y. Grigoryev, E. M. Sulman, M. B. Konyaeva and V. G. Matveeva, *J. Phys. Chem. A*, 2013, **117**, 4073–4083.
- 32 D. K. Mishra, A. A. Dabbawala, J. J. Park, S. H. Jung and J.-S. Hwang, *Catal. Today*, 2014, **232**, 99–107.
- 33 A. Aho, S. Roggan, K. Eränen, T. Salmi and D. Y. Murzin, *Catal. Sci. Technol.*, 2015, **5**, 953–959.
- 34 A. Aho, S. Roggan, O. A. Simakova, T. Salmi and D. Y. Murzin, *Catal. Today*, 2015, **241**, 195–199.
- 35 P. A. Lazaridis, S. Karakoulia, A. Delimitis, S. M. Coman, V. I. Parvulescu and K. S. Triantafyllidis, *Catal. Today*, 2015, **257**, 281–290.
- 36 A. A. Dabbawala, D. K. Mishra and J.-S. Hwang, *Catal. Today*, 2016, **265**, 163–173.
- 37 J. A. Melero, J. Moreno, J. Iglesias, G. Morales, J. L. G. Fierro, R. Sánchez-Vázquez, A. Cubo and B. García, *Mol. Catal.*, 2020, **484**, 110802.
- 38 A. Perrard, P. Gallezot, J.-P. Joly, R. Durand, C. Baljou, B. Coq and P. Trens, *Appl. Catal. A*, 2007, **331**, 100–104.
- 39 X. Zhang, L. J. Durndell, M. A. Isaacs, C. M. A. Parlett, A. F. Lee and K. Wilson, *ACS Catal.*, 2016, **6**, 7409–7417.
- 40 D. Shi, R. Wojcieszak, S. Paul and E. Marceau, *Catalysts*, 2019, **9**, 451.
- 41 B. W. Hoffer, E. Crezee, F. Devred, P. R. M. Mooijman, W. G. Sloof, P. J. Kooyman, A. D. van Langeveld, F. Kapteijn and J. A. Moulijn, *Appl. Catal. A*, 2003, **253**, 437–452.
- 42 A. Romero, A. Nieto-Márquez and E. Alonso, *Appl. Catal. A*, 2017, **529**, 49–59.
- 43 N. Déchamp, A. Gamez, A. Perrard and P. Gallezot, *Catal. Today*, 1995, **24**, 29–34.
- 44 S. Fujita, K. Nakajima, J. Yamasaki, T. Mizugaki, K. Jitsukawa and T. Mitsudome, *ACS Catal.*, 2020, **10**, 4261–4267.
- 45 A. L. Ankudinov, B. Ravel, J. J. Rehr and S. D. Conradson, *Phys. Rev. B*, 1998, **58**, 7565–7576.
- 46 C. Wu and P. T. Williams, *Environ. Sci. Technol.*, 2010, **44**, 5993–5998.
- 47 B. Malleshham, P. Sudarsanam, B. V. S. Reddy, B. G. Rao and B. M. Reddy, *ACS Omega*, 2018, **3**, 16839–16849.
- 48 Y. Pan, Y. Liu, J. Zhao, K. Yang, J. Liang, D. Liu, W. Hu, D. Liu, Y. Liu and C. Liu, *J. Mater. Chem. A*, 2015, **3**, 1656–1665.
- 49 M. Yabushita, N. Shibayama, K. Nakajima and A. Fukuoka, *ACS Catal.*, 2019, **9**, 2101–2109.
- 50 C. Miao, T. Hui, Y. Liu, J. Feng and D. Li, *J. Catal.*, 2019, **370**, 107–117.